Review of the Discrete Changes Model of Intercore Crosstalk in Weakly-coupled Multicore Fibers

Adolfo V. T. Cartaxo, Tiago M. F. Alves and João L. Rebola
Instituto de Telecomunicações, Lisbon 1049-001, Portugal
ISCTE - Instituto Universitário de Lisboa, Lisbon 1649-026, Portugal
Tel: +351 217 650 598, e-mail: adolfo.cartaxo@lx.it.pt

ABSTRACT
We review the discrete changes model (DCM) of intercore crosstalk (ICXT) in weakly-coupled multicore fiber systems. The stochastic time evolution, decorrelation bandwidth and polarization fluctuations over time of the ICXT are analysed numerically and experimentally. The DCM limitations and advantages are highlighted.
Keywords: decorrelation bandwidth, decorrelation time, discrete changes model, intercore crosstalk, polarization fluctuations, weakly-coupled multicore fiber

1. INTRODUCTION

Weakly-coupled multicore fibers (WC-MCFs) have been proposed to overcome the capacity crunch foreseen for the near future in next generation optical networks [1]. The intercore crosstalk (ICXT) can be an important impairment in WC-MCF based networks and becomes far more relevant for WC-MCFs with higher core count and shorter core-to-core distance [1]. ICXT in WC-MCFs varies randomly over the longitudinal direction of the fiber, and over time and frequency [2], [3]. The time variation of the ICXT may lead to significant fluctuations of the system performance and result in critical outage probabilities [4], [5]. Depending on the magnitude of the ICXT decorrelation bandwidth relative to the bandwidth of the data signal, the frequency dependence of the ICXT may lead to a static or a dynamic ICXT effect [6], [7].

Among several proposed ICXT models [2], [8]-[10], the discrete changes model (DCM) is particularly interesting for ICXT simulation and characterization because it reduces complexity and simulation time to an acceptable level, and takes into account specific fiber properties (such as core refractive index, index profile, core radius, pitch) and longitudinal bending and twisting perturbations of the WC-MCF. To describe the ICXT more accurately, the DCM has evolved and different flavours of the DCM have been proposed [2], [3], [7], [11]-[16]. They all rely on the fact that the ICXT field results mostly from field contributions induced at the phase-matching points (PMPs), i. e. the points along the longitudinal coordinate of the MCF for which the difference between the effective refractive indexes of the interfering and interfered cores is zero. The range of bending radius and effective intrinsic refractive indexes for which PMPs exist define the so-called phase-matching region (PMR). The DCM was originally proposed for homogeneous WC-MCFs [2], [11] and later generalized to real homogeneous WC-MCFs, i. e. WC-MCFs whose cores have similar but not exactly the same refractive indexes [12]. The original DCM has been improved to include the dependence on the modulation frequency [3], [7], the difference between the dispersion parameters of the cores [13], dual-polarization [14], and the random time nature of ICXT [15], [16].

In this work, we review and provide an integrated view of the DCM that describes the stochastic time evolution, decorrelation bandwidth and polarization fluctuations over time of the ICXT.

2. DUAL POLARIZATION DCM WITH TIME AND FREQUENCY DEPENDENCE

In the DCM, the ICXT field induced by the interfering core m at the output of the interfered core n results from a discrete sum of N_p contributions associated with N_p PMPs [2], [11]. Each one of these contributions is weighted by a random phase shift (RPS), due to the effect of slight random fluctuations in the bending radius, twisting rate, and other fibre parameters on the propagation constant [2], [11], and delayed by the skew between the interfering and interfered cores after propagation up to the longitudinal coordinate of k-th center point between consecutive PMPs, $z_m^{(k)}$ [3], [16]. As each PMP is located at a different longitudinal coordinate, the delay differs from one contribution to another. The stochastic time dependence of the ICXT was incorporated relying on the fact that, in the original DCM, the whole randomness of ICXT is included in the RPSs and, hence, an intuitive explanation for the stochastic time dependence of ICXT is to attribute time dependence to the RPSs [15]-[16]. The models proposed for the time dependence of the RPSs (detailed in the following) have been already proposed to describe the time dependence of other random effects in optical components, e .g. fiber birefringence and laser phase noise. The generalization of the original DCM to dual polarization relies on that, for sufficiently long MCFs: (i) due to random polarization mixing, the mean ICXT power of each polarization and the total of the two polarizations, at the MCF output, is the same regardless the power distribution at the MCF input; (ii) the in-phase and quadrature components of the two polarizations are uncorrelated [14]. Figure 1 shows a simplified scheme of the ICXT generation, where $h_{n,m}^{(k)}(t)$ describes the change of the ICXT field due to the k-th RPS.

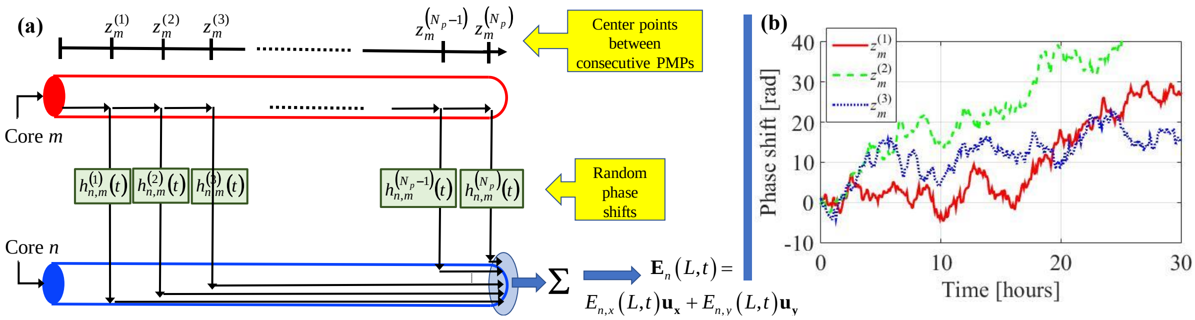

Figure 1. (a) Simplified scheme of the ICXT generation along the WC-MCF. (b) Samples of the RPSs associated with the first three PMPs along the WC-MCF for a decorrelation time of 5 minutes.

For linear propagation along the WC-MCF with N_c cores, neglecting the core loss and considering the random coupling between polarizations along the fiber, the slowly varying complex amplitude of the ICXT electric field of the interfered core n at the MCF output is given by [7], [16]

$$\begin{aligned} &x\text{-pol. component:} \quad E_{n,x}(L,t) = -j\sum_{\substack{m=1\\m\neq n}}^{N_c}\frac{\bar{K}_{nm}}{\sqrt{2}}\sum_{k=1}^{N_p}\left(F_{nm,x}^{(k)}\left(0,t-\bar{\varsigma}_{nm}^{(k)}\right)v_{1,nm}^{(k)}(t)+F_{nm,y}^{(k)}\left(0,t-\bar{\varsigma}_{nm}^{(k)}\right)v_{2,nm}^{(k)}(t)\right) \\ &y\text{-pol. component:} \quad E_{n,y}(L,t) = -j\sum_{\substack{m=1\\m\neq n}}^{N_c}\frac{\bar{K}_{nm}}{\sqrt{2}}\sum_{k=1}^{N_p}\left(F_{nm,x}^{(k)}\left(0,t-\bar{\varsigma}_{nm}^{(k)}\right)v_{3,nm}^{(k)}(t)+F_{nm,y}^{(k)}\left(0,t-\bar{\varsigma}_{nm}^{(k)}\right)v_{4,nm}^{(k)}(t)\right) \end{aligned} \tag{1}$$

where L is the MCF length, t is the time, $\bar{K}_{nm}$ is the discrete coupling coefficient evaluated from the average of the intercore coupling coefficients (between cores n and m) of the two orthogonal polarization directions $\mathbf{u_x}$ and $\mathbf{u_y}$, which may be slightly different due to the birefringence effect [9], $\bar{K}_{nm} = 0.5\times\left(\bar{K}_{nm,x}+\bar{K}_{nm,y}\right)$, and

$$\begin{aligned} &v_{i,nm}^{(k)}(t) = \exp\left[-j\left(\Theta_{i,m}^{(k)}(t)+\bar{\varphi}_{nm}^{(k)}\right)\right]; \qquad F_{nm,(x,y)}^{(k)}(0,t) = \mathrm{FT}^{-1}\left[\tilde{E}_{m,(x,y)}(0,\omega)\exp\left(-j\bar{\eta}_{nm}^{(k)}\omega^2\right)\right] \\ &\bar{\varphi}_{nm}^{(k)} = \bar{\beta}_{n,0}\left(L-z_m^{(k)}\right)+\bar{\beta}_{m,0}z_m^{(k)}; \quad \bar{\varsigma}_{nm}^{(k)} = \bar{\beta}_{n,1}\left(L-z_m^{(k)}\right)+\bar{\beta}_{m,1}z_m^{(k)}; \quad \bar{\eta}_{nm}^{(k)} = \bar{\beta}_{n,2}\left(L-z_m^{(k)}\right)+\bar{\beta}_{m,2}z_m^{(k)} \end{aligned} \tag{2}$$

where ω is the angular frequency, $\mathrm{FT}^{-1}[\cdot]$ is the inverse Fourier transform operator, $\bar{\beta}_{q,i}$ is the average of the i-th order derivative of the intrinsic propagation constant of core q (n or m) of the two polarizations with respect to angular frequency. The functions $v_{i,nm}^{(k)}(t)$ represent the coupling between the orthogonal polarization directions [14, 16]. $\tilde{E}_{m,(x,y)}(0,\omega)$ is the Fourier transform of the ICXT field at the input of core m in the x or y polarization direction. $\Theta_{i,m}^{(k)}(t)$ are independent random processes that model the time varying RPSs associated with each PMP of the m-th interfering core. $\Theta_{i,m}^{(k)}(t)$ have been modelled as i) independent, stationary Brownian motions [15] and ii) independent non-stationary Wiener processes [16]. Better agreement with experimental data has been obtained considering the Wiener process [16]. In this case, $\Theta_{i,m}^{(k)}(t) = 2\pi\int_0^t \mu_{i,m}^{(k)}(\tau)d\tau$, with $t>0$, where $\mu_{i,m}^{(k)}(t)$ is the first order time derivative of the phase shift associated with each PMP of the m-th interfering core. Hence, $\mu_{i,m}^{(k)}(t)$ is a zero mean white Gaussian noise process with double sided power spectral density given by $S_m = 1/\left(4\pi^2 T_{XT,m}\right)$, where $T_{XT,m}$ is the decorrelation time at $1/e$ of the ICXT generated in core n by the interfering core m. This model holds also for heterogeneous WC-MCF operating in the phase matching region, with $\bar{K}_{nm}$ in (1) replaced by $\bar{K}'_{nm}$ with $\bar{K}'_{nm} = 0.5\times\left(\bar{K}_{nm}+\bar{K}_{mn}\right)$. The dependence of $\bar{K}_{nm}$ on the WC-MCF properties (e. g. core refractive index and profile, core radius, pitch) can be found in eqs. (28) and (29) in [12].

The DCM given by eq. (1) allows to consider an arbitrary signal in core m inducing the ICXT in core n by setting $\tilde{E}_{m,(x,y)}(0,\omega)$ adequately. In the particular case of a continuous wave (CW) signal with zero linewidth at the input of core m, the mean power of the ICXT evaluated from eq. (1) is $\mathrm{E}\left[\left|E_{n,x}(L,t)\right|^2+\left|E_{n,y}(L,t)\right|^2\right] = N_p\left|\bar{K}_{nm}\right|^2$, where E[$x$] is the expected value of x.

3. RESULTS AND DISCUSSION

The ICXT has been usually characterized from measurements using a power meter [3], [15], [16], firstly considering CW sources at the interfering core input and later considering modulated sources [17]. The use of the power meter provides assessment of the short term average crosstalk (STAXT), which is usually different from the instantaneous ICXT power. For the typical decorrelation times of ICXT (a few or more minutes), only in particular cases, e. g., CW source with coherence time much higher than the intercore skew, the STAXT provides a good estimate of the instantaneous ICXT power.

Using the DCM presented in section 2, the stochastic time evolution of STAXT in WC-MCFs with multiple interfering cores was studied considering a CW source with coherence time much higher than the intercore skew at the interfering core input [16]. Therein, general expressions for the STAXT autocovariance and decorrelation time estimated from the DCM were presented and compared with experimental results of a WC-MCF with 19 cores and skew between pair of cores ranging from 2 to 7 ns using an external cavity laser with linewidth of about 100 kHz. Further details on the STAXT decorrelation time experiments can be found in [16]. The inset of Figure 2-(a) shows a sample of the measured STAXT along 50 hours with 6 interfering cores, where peak-to-peak fluctuations exceeding 15 dB can be seen. Figure 2-(a) presents results that illustrate the level of agreement achieved by the DCM with experimental results. Those results refer to the autocovariance of the STAXT generated by 6 interfering cores. Firstly, a similar fitting was achieved when testing each one of interfering cores (out of the six interfering cores), and was used to estimate the decorrelation time between each pair of cores. Decorrelation times between 2.6 and 4 minutes were estimated. Using those estimated decorrelation times, the theoretical prediction of STAXT autocovariance shown in Fig. 2-(a) is obtained. The decorrelation time of the STAXT evaluated experimentally with six interfering cores is 2.7 minutes which is of the same order of magnitude of the decorrelation time of the STAXT obtained for each pair of cores, and exceeds the one obtained for the pair of cores with shorter decorrelation time.

An important issue related to the estimation of the decorrelation time is the elapsed time required to get stabilized estimates of the decorrelation time experimentally. Figure 2-(b) shows the estimate of decorrelation time for two pairs of cores (similar results were also obtained for the other pairs) as a function of the elapsed time considered to estimate the decorrelation time. That figure shows that 100 hours are required to get stabilized estimates of decorrelation times of the order of a few minutes. For these decorrelation times, more than 20 hours were also required to get stabilized estimates of mean STAXT (fluctuations lower than 1 dB).

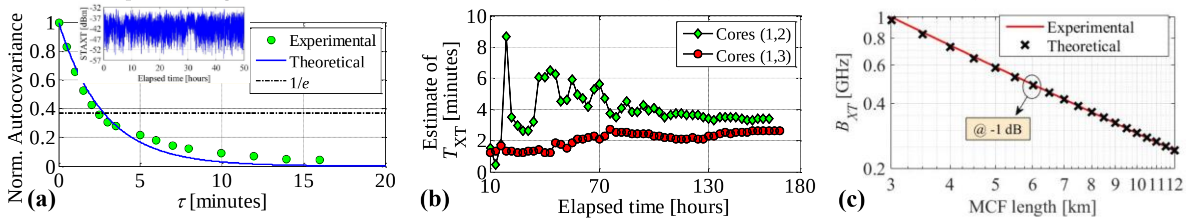

Figure 2. (a) Autocovariance of the ICXT generated by 6 interfering cores (inset: sample of measured STAXT). (b) Decorrelation time of the ICXT measured experimentally at the output of the central core as function of the elapsed time with a single interfering core. (c) Decorrelation bandwidth of the ICXT as a function of the MCF length with a single interfering core with walk-off of 90 ps/km.

Using the DCM presented in section 2, the equivalent autocovariance function of the ICXT power that enables evaluating the correlation between the ICXT power generated at two different frequencies by WC-MCFs with multiple interfering cores was assessed theoretically [7]. Theoretical estimates of the decorrelation bandwidth provided by a closed-form expression were compared with experimental data [7]. Figure 2-(c) presents results that illustrate the level of agreement achieved by the DCM with experimental results. Those results refer to the decorrelation bandwidth of the ICXT measured as a function of the MCF length with a single interfering core with walk-off of 90 ps/km. In this figure, the decorrelation bandwidth was defined as the frequency lag corresponding to −1 dB of the maximum of the autocorrelation of the ICXT spectrum. It was found theoretically to be one fourth of the inverse of the skew between cores [7]. The experimental results shown in Figure 2-(c) were extracted from [18]. Excellent agreement between theoretical and experimental results is shown. Those analyses provide relevant information about the decorrelation bandwidth of the ICXT induced in MCFs with multiple interfering cores to be used to assist the design of next generation MCF-based systems.

Recently, the impact of randomly changing polarization of ICXT on the performance was highlighted as an important issue in WC-MCF systems [19]. In order to assess the evolution of the polarization along time predicted by the DCM presented in section 2, a CW signal without phase noise was considered at the interfering core input and the Stokes parameters were evaluated numerically. The consideration of absence of phase noise allows to attribute the observed behaviour of the polarization along time only to ICXT mechanism and not to phase noise either. In Fig. 3, we show the evolution of the polarization state of ICXT on the Poincaré sphere (with sampling interval of 1 s) for decorrelation times of 30 minutes and 3 minutes and monitoring periods with duration of 1 and 60 minutes, for a WC-MCF with intercore skew of 4 ns. While, for short monitoring periods, the polarization state shows a small variation, for monitoring periods much longer than the decorrelation time, almost all polarization states tend to be visited. Therefore, the DCM provides a qualitative good description of the ICXT as for long monitoring periods it is expected that the ICXT polarization state varies significantly, as already reported in [19]. This subject requires further study.

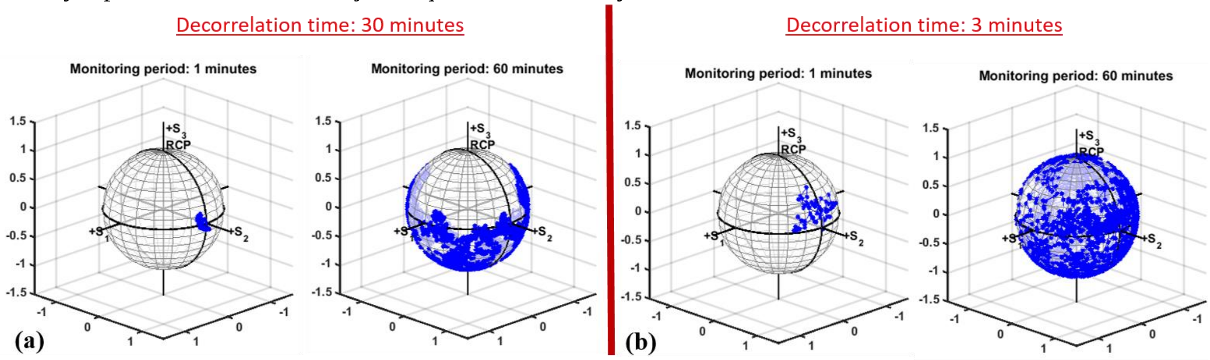

Figure 3. Evolution of polarization state of ICXT on the Poincaré sphere with decorrelation time of 30 minutes (a) and 3 minutes (b) along monitoring periods with duration of 1 and 60 minutes.

4. CONCLUSIONS

The main reasons for the interest in the dual polarization DCM with time and frequency dependence is its straightforward numerical implementation, reasonably accurate stochastic description of the ICXT along time and frequency, and very quick ICXT estimates when compared to the estimates obtained by solving the coupled-mode equations numerically. However, the DCM is only valid in the PMR. Therefore, the application of the DCM in several interesting situations corresponding to the non-PMR may be questionable.

ACKNOWLEDGEMENTS

Fundação para a Ciência e a Tecnologia (FCT) from Portugal under the project UIDB/EEA/50008/2020.

REFERENCES

[1] B. Puttnam *et al*.: High capacity transmission systems using homogeneous multi-core fibers, *J. Lightwave Technol.*, vol. 35, pp. 1157-1167, 2017.
[2] T. Hayashi, *et al*.: Crosstalk variation of multi-core fibre due to fibre bend, in *Proc. ECOC*, Turin, Italy, Sep. 2010, paper We.8.F.6.
[3] R. Luís *et al*.: Time and modulation frequency dependence of crosstalk in homogeneous multi-core fibers, *J. Lightwave Technol.*, vol. 34, no. 2, pp. 441–447, Jan. 2016.
[4] T. Alves *et al*.: Performance of adaptive DD-OFDM multicore fiber links and its relation with intercore crosstalk, *Opt. Express*, vol. 25, pp. 16017-16027, 2017.
[5] J. Rebola, *et al*.: Outage probability due to intercore crosstalk in dual-core fiber links with direct-detection, *IEEE Photon. Technol. Lett*., DOI: 10.1109/LPT.2019.2921934, 2019.
[6] T. Hayashi, T. Sasaki, and E. Sasaoka: Behaviour of inter-core crosstalk as a noise and its effect on Q-factor in multi-core fiber, *IEICE Trans. Commun.*, vol. E97-B, no. 5, pp. 936–944, 2014.
[7] T. Alves and A. Cartaxo: Decorrelation bandwidth of intercore crosstalk in weakly coupled multicore fibers with multiple interfering cores, *J. Lightwave Technol.*, vol. 37, pp. 744–754, 2019.
[8] M. Koshiba, *et al*.: Analytical expression of average power-coupling coefficients for estimating intercore crosstalk in multicore fibers, *IEEE Photon. J.*, vol. 4, no. 5, pp. 1987–1995, Oct. 2012.
[9] A. Macho, *et al*.: Birefringence effects in multi-core fiber: coupled local-mode theory, *Opt. Express*, vol. 24, pp. 21415–21434, 2016.
[10] S. Mumtaz, R.-J. Essiambre, and G. Agrawal: Nonlinear propagation in multimode and multicore fibers: generalization of the Manakov equations, *J. Lightwave Technol.*, vol. 31, no. 3, pp. 398–406, Jan. 2013.
[11] T. Hayashi, *et al*.: Design and fabrication of ultra-low crosstalk and low-loss multi-core fiber, *Opt. Express*, vol. 19, pp. 16576–16592, Aug. 2011.
[12] A. Cartaxo and T. Alves: Discrete changes model of inter-core crosstalk of real homogeneous multi-core fibers, *J. Lightwave Technol.*, vol. 35, pp. 2398–2408, Jun. 2017.
[13] A. Cartaxo, *et al*.: Dispersion impact on the crosstalk amplitude response of homogeneous multi-core fibers, *IEEE Photon. Technol. Lett*., vol. 28, pp. 1858–1861, Sep. 2016.
[14] R. Soeiro, T. Alves, and A. Cartaxo: Dual polarization discrete changes model of inter-core crosstalk in multi-core fibers, *IEEE Photon. Technol. Lett*., vol. 29, pp. 1395–1398, 2017.
[15] T. Alves and A. Cartaxo: Intercore crosstalk in homogeneous multicore fibers: theoretical characterization of stochastic time evolution, *J. Lightwave Technol.*, vol. 35, pp. 4613–4623, Nov. 2017.
[16] T. Alves and A. Cartaxo: Characterization of the stochastic time evolution of short-term average intercore crosstalk in multicore fibers with multiple interfering cores, *Opt. Express*, vol. 26, pp. 4605–4620, Feb. 2018.
[17] T. Alves, A. Cartaxo and J. Rebola: Stochastic properties and outage in crosstalk-impaired OOK-DD weakly-coupled MCF applications with low and high skew×bit-rate, *IEEE J. Sel. Topics Quantum Electronics*, doi: 10.1109/JSTQE.2020.2995306, 2020.
[18] L. Gan *et al*.: Investigation of channel model for weakly coupled multicore fiber, *Opt. Express*, vol. 26, pp. 5182–5199, 2018.
[19] G. Rademacher, *et al*.: Crosstalk induced system outage in intensity modulated direct-detection multi-core fiber transmission, *J. Lightwave Technol.*, vol. 38, pp. 291-296, 2020.